applied sciences

MDPI

Article

Two- and Three-Photon Partial Photoionization Cross Sections of Li^+, Ne^{8+} and Ar^{16+} under XUV Radiation

William Hanks, John T. Costello and Lampros A.A. Nikolopoulos *

School of Physical Sciences, Dublin City University, Dublin 9, Ireland; william.hanks2@mail.dcu.ie (W.H.); John.costello@dcu.ie (J.T.C.)

* Correspondence: Lampros.Nikolopoulos@dcu.ie; Tel.: +353-1-7005-300

Academic Editor: Kiyoshi Ueda

Received: 14 February 2017; Accepted: 9 March 2017; Published:17 March 2017

Abstract: In this work, we present the photon energy dependence of the two- and three-photon cross sections of the two-electron Li^+, Ne^{8+} and Ar^{16+} ions, following photoionization from their ground state. The expressions for the cross sections are based on the lowest-order (non-vanishing) perturbation theory for the electric field, while the calculations are made with the use of an ab initio configuration interaction method. The ionization cross section is dominated by pronounced single photon resonances in addition to peaks associated with doubly excited resonances. In the case of two-photon ionization, and in the non-resonant part of the cross section, we find that the ^1D ionization channel overwhelms the ^1S one. We also observe that, as one moves from the lowest atomic number ion, namely Li^+, to the highest atomic number ion, namely Ar^{16+}, the cross sections generally decrease.

Keywords: multiphoton ionization; X-ray radiation; free-electron laser; lowest-order perturbation theory; cross sections

1. Introduction

During the last decade, the advent of new light sources, capable of delivering intense and/or ultrashort, coherent radiation in the soft- and hard-X-ray regime, either directly by free-electron lasers (FEL) or indirectly by high-harmonic generation techniques, has renewed interest in experimental and theoretical photoionization studies of multiply charged ions. The excitation of atoms/molecules involving inner-shell electrons with such light sources offers the possibility of investigating processes at their natural time-scale, such as Auger processes and its variations [1], double core-hole creation and ionization [2], resonant enhanced photoionization, etc. Beyond the viewpoint of accessing the dynamics of these processes, the availability of extremely high flux has made it feasible to experimentally create the required conditions and observe for the first time new processes, for example the two-photon single- and double-(direct) photoionization of helium, the complete stripping of neon [3] and multiphoton inner-shell ionization in noble gases [4] and solid targets [5]. Since a number of recent reviews elaborate on experimental and theoretical studies as well as on their numerous applications in this short wavelength regime [6–9], we will only mention here that typical fluxes of FELs to date range between 5×10^{11} Wcm^{-2} to 5×10^{18} Wcm^{-2}, photon energies range in (0.02–15) KeV, while average full width at half maximum (FWHM) durations vary from 10 fs to 85 fs. It is also worth noting that three new FELs are under development and set to start user operations soon (E-XFEL, Swiss FEL, PAL) with extra pulse parameter specifications compared to the current ones. Notably, the Swiss FEL will provide pulses as short as 2 fs while E-XFEL as long as 100 fs with a repetition rate between 50–100 times higher than any other existing FEL.

From the above discussion, it appears that, nowadays, in these wavelength regimes, excitation/ionization processes involving more than one photon are routinely feasible. Accordingly, their quantitative description requires theoretical approaches capable of coping with the non-linear features of the interaction between X-ray radiation with atomic and molecular systems. Amongst the various theoretical approaches, one is based on a perturbation expansion of the interaction potential with respect to the electric field, known as lowest-order (non-vanishing) perturbation theory (LOPT) [10]. In the case of X-ray quasi-monochromatic radiation, the use of LOPT is well justified for the current available peak intensities. The main requirements are for (a) the ponderomotive potential, $V_p = I_0/4\omega^2$, and (b) the bandwidth, $\Delta\omega$, to be much smaller than the mean central photon frequency, ω, of the radiation. For our case, for example, if we choose a peak intensity at the higher end, $I_0 \simeq 3.51 \times 10^{18}$ W/cm^2, and a mean photon energy at the lowest limit of soft X-ray spectrum, say $\omega \sim 270$ eV, then $V_p/\omega \simeq 0.025 << 1$. Since for current FEL sources the bandwidth, $\Delta\omega$, ranges in $(10^{-3}$–$10^{-2})\omega$, LOPT is very well suited to provide reliable quantitative information about various quantities of experimental interest, for example, ion and fluorescence yields.

The validity of LOPT to calculate few X-ray photon processes allows the development of an alternative theoretical framework in place of the direct, but much more demanding, integration of a multielectron time-dependent Schrödinger equation. In the present work, we have chosen to apply LOPT to three elements of high experimental interest, namely Li, Ne and Ar. As it is known, these three atomic elements have been the subject of numerous experiments and theoretical studies since the inception of quantum mechanics. Excitation and ionization of the valence shells of the neutral species of these elements have been extensively studied and experimental reports and theoretical calculations about their photoionization cross sections are available in literature. In contrast to this plethora of data, the availability of analogous studies of their ionized species are scarce, especially when few-photon ionization is involved. To provide one example illustrating the need for such data, we mention the case of neon's multiple ionization in the pioneering experiment of Young et al. [3] at LCLS with a FEL pulse at a photon energy circa 1110 eV (pulse peak intensity and FWHM duration were estimated to be 10^{17} W/cm^2 and 100 fs, respectively). In this experiment, the ionization of Ne^{8+}, following the sequential one-photon stripping of the lower charged neon ions, proceeds mainly through a two-photon absorption (the ionization potential of Ne^{8+} is circa 1362 eV). It is needless to say that the same two-photon ionization channel would have been the dominant ionization channel for any photon in the energy range between 681 eV $\leq \omega \leq$ 1362 eV; thus, the need for two-photon ionization cross sections for a range of photon energies. Of course, similar considerations can be carried over to any atomic system and of any degree of charge in the presence of X-ray radiation.

In the simplest case of the one-electron charged ions, multiphoton cross sections can be straightforwardly calculated by scaling the corresponding hydrogen cross sections according to the relation $\sigma_N(Z^2\omega) = \sigma_N^{(H)}/Z^{4N-2}$ [11], where $\sigma_N^{(H)}$ is the N-photon cross section of hydrogen and Z is the atomic number of the element. Throughout the years, a number of reports have appeared in literature with multiphoton cross sections of hydrogen involving quite a high number of photons as, for example, the calculations by Karule [12] and by Potvliege and Shakeshaft (N = 20) [13]. Next in line are charged ions with only their K-shell electrons remaining, making them helium-like (two-electron) systems. For helium, systematic studies exist where two, three- and four-photon LOPT ionization cross sections are calculated [14]; it appears, despite the significance of Li, Ne and Ar as experimental and theoretical targets, that no similar detailed study has been extended to these systems. To the best of our knowledge, we are aware of the two- and three-photon total ionization cross sections that have been calculated on Li^+ with the use of single-channel quantum-defect theory (SQDT) [15], the work of Novikov and Hopersky in neon ions [16], the more recent work by the group of R. Santra [17] (Ne^{8+}) and the two-photon total cross sections on Ne^{8+} and Ar^{16+}, obtained through a Greens-function method calculation [18].

More specifically, in the present study, we apply an ab initio configuration interaction (CI) approach and make use of LOPT to calculate the two- and three-photon partial photoionization cross

sections for Li^+, Ne^{8+} and Ar^{16+}. In addition to this, we have calculated details of their electronic structure. The structure of the text is as follows: in Section 2, we present the theoretical method in sufficient detail for a self-contained formulation of the present study; in Section 3, we present and discuss our results about the calculated energies and the LOPT two- and three-photon ionization partial cross sections. Finally, we conclude with a summary of our findings and a brief discussion of possible further investigations within the present context. In the presentation of the theoretical formulas, we use the atomic-Gaussian unit system ($\hbar = m_e = e = 1/4\pi\varepsilon_0 = 1$). In the figures, the cross sections and the energies are presented in more traditional units, namely, eV for the energies, and cm^4s and cm^6s^2 for the two- and three-photon cross sections, respectively.

2. Theoretical Formulation

The chosen ions have the common feature in that they only have two-electrons, thus allowing a fully ab initio calculation of their atomic structure. The calculation proceeds in two stages. First, we follow a configuration interaction method to calculate the eigenstates and the associated bound and continuum states of these systems, and then we apply LOPT to obtain a generalized multiphoton cross section that can, in turn, be used to calculate two- and three-photon cross sections. These steps are described in greater detail below. Although the computational procedure has been presented in detail in a number of articles [19–23], it is necessary to include some brief presentation, adjusted to the particular case of ionization by linearly polarized X-ray radiation. The latter property of the radiation and the fact that the ground state of the ions, $^1S_0$, is spherically symmetric, combined with the selection rules for electric dipole interactions, restricts the states to those of singlet-symmetry with a total magnetic quantum number value of zero. We take advantage of this from the outset in order to simplify the formulation.

2.1. Atomic Structure Calculation

The non-relativistic two-electron ionic Hamiltonian, H_A, in atomic units, is given by:

$$\hat{H}_A = \hat{h}(\mathbf{r}_1) + \hat{h}(\mathbf{r}_2) + \frac{1}{|\mathbf{r}_1 - \mathbf{r}_2|}, \tag{1}$$

where $\hat{h}(\mathbf{r}_i) = -\nabla_i^2/2 - Z/r_i$ and $\mathbf{r}_i$, $i = 1, 2$, denotes each electron's coordinate. $-\nabla_i^2/2$ represents the electronic kinetic energy operator, $-Z/r_i$ the nucleus-i^{th} electron electrostatic (Coulombic) potential (where it is assumed that the nucleus defines the origin of the working coordinate system) and $1/|\mathbf{r}_1 - \mathbf{r}_2|$ represents the corresponding inter-electronic electrostatic potential. Z is the atomic number, which is 3 for Li^+, 10 for Ne^{8+} and 18 for Ar^{16+}.

First, we numerically solve the Schrödinger equation (SE), $(\hat{h}(\mathbf{r}) - \epsilon)\phi_{\epsilon l m_l}(\mathbf{r}) = 0$, for the mono-electronic systems Li^{2+}, Ne^{9+} and Ar^{17+}. To this end, we adopt a separation of variables approach where the one-electron orbitals are expressed as $\phi_{\epsilon l m_l}(\mathbf{r}) = [P_\epsilon(r)/r]Y_{l m_l}(\theta, \phi)$ where $Y_{l m_l}(\theta, \phi)$, are the spherical harmonic functions. Projection of $\phi_{\epsilon l m_l}(\mathbf{r})$ onto the one-electron SE, followed by angular integration leads to the one-dimensional radial differential equation for the unknown radial orbitals, $P_\epsilon(r)$:

$$\left[-\frac{1}{2}\frac{d^2}{dr^2} + \frac{l(l+1)}{2r^2} - \frac{Z}{r} - \epsilon\right] P_\epsilon(r) = 0. \tag{2}$$

The present method assumes that the radial configuration space of the electron is limited to a finite radius, R, with the boundary conditions chosen as: $P_\epsilon(0) = P_\epsilon(R) = 0$. The immediate consequence of this assumption is to allow for a finite matrix representation of the physical Hamiltonian with a discretized eigenergy spectrum including both the bound ($\epsilon < 0$) and the continuum eigenstates ($\epsilon > 0$). Moreover, we also see that both the eigenenergies and eigenstates are dependent on the particular angular momentum number, l. In the following, we adopt the following discretized notation

for the eigenvalues and the eigenfunction: $\varepsilon \to \varepsilon_{nl}$ and $P_\epsilon(r) \to P_{nl}$. The positive-energy eigenstates, $\varepsilon_{nl} \geq 0$, exhibit oscillatory asymptotic behaviour, similar to that expected from continuum-like eigenstates. On the other hand, the negative-energy eigenstates, $\varepsilon_{nl} < 0$, have an exponentially decaying asymptotic behaviour associated with the bound spectrum of the finite Hamiltonian. The numerical solution then proceeds by expanding the radial orbitals, $P_{nl}(r) = \sum_i c_i^{(nl)} B_i^{(k_b)}(r)$, on a nonorthogonal set of B-spline polynomials of order k_b and total number n_b defined in the finite interval $[0, R]$ [24]. The particular choice of a B-spline basis, as opposed to a Gaussian or Slater-type basis, is dictated by their superior ability to represent the continuum solutions with great accuracy. This expansion leads to a diagonalization matrix problem, where the solution provides the unknown coefficients, $c_i^{(nl)}$ [25].

Having calculated the radial orbitals, $P_{nl}(r)$, for each partial wave $l = 0, 1, 2, ...$, we proceed with the solution of the SE for the two-electron ions Li^+, Ne^{8+} and Ar^{16+}:

$$\hat{H}_A \Psi_{EL}(\mathbf{r}_1, \mathbf{r}_2) = E_L \Psi_{EL}(\mathbf{r}_1, \mathbf{r}_2). \tag{3}$$

The calculational method proceeds along similar lines to the one-electron case. We shall expand the two-electron eigenstates, Ψ_{EL} (*configuration interaction, CI basis*), on a known two-electron basis set (*configuration basis*), $\Phi_a^{(L)}(\mathbf{r}_1,\mathbf{r}_2)$:

$$\Psi_{EL}(\mathbf{r}_1, \mathbf{r}_2) = \sum_a C_a^{(EL)} \Phi_a^{(L)}(\mathbf{r}_1,\mathbf{r}_2), \tag{4}$$

with the intention to express Equation (3) as an alegbraic equation for the C_a^{EL} coefficients. We choose as configuration states, the eigenstates of the $\hat{H}_A^{(0)}, \mathbf{L}^2, \hat{L}_z, \mathbf{S}^2, \hat{S}_z$, and $\hat{\Pi}$ (parity) operators, where $\hat{H}_A^{(0)} = \hat{h}(\mathbf{r}_1) + \hat{h}_2(\mathbf{r}_2)$, $\hat{L} = \hat{l}_1 + \hat{l}_2$ and $\hat{S} = \hat{s}_1 + \hat{s}_2$. $\hat{l}_i$ and $\hat{s}_i$ are the i^{th} electron's angular and spin quantum operators, respectively. $\hat{H}_A^{(0)}$ is the so-called zero-order two-electron Hamiltonian (of a physically fictitious system where the two-electrons are non-interacting), $\hat{L}$ is the total angular momentum operator, $\hat{L}_z$ is its projection onto the quantization axis (chosen to be the z-axis), and $\hat{S}$, $\hat{S}_z$ are the total spin quantum number and its z-axis projection, respectively. The CI states in Equation (4) are characterized only by their energy, E, and total angular quantum number, L, on the basis that the interaction with the field will not affect the total magnetic quantum number, M_L, as well as the total spin, S, and its z-axis projection, M_S. These values will be equal to those of the initial state. For two electron systems, known to have a ^1S ground state, it is concluded that only states with $M_L = 0$, $S = 0$ and $M_S = 0$ are involved in the photoionization process. Accordingly, the zero-order states are fully determined if the set of L and $a \equiv (n_1 l_1; n_2 l_2)$ parameters is given. The respective zero-order energy is equal to $E_0 = \epsilon_1 + \epsilon_2$. Therefore, the configuration basis set is comprised of singlet ($S = 0$), spatially antisymmetric, angularly coupled, products of one-electron orbitals with $m_l = 0$:

$$\Phi^{(L)}_{n_1 l_1; n_2 l_2}(\mathbf{r}_1, \mathbf{r}_2) = C_{000}^{l_1 l_2 L} \hat{A}_{12} \left[\phi_{n_1 l_1}(\mathbf{r}_1) \phi_{n_2 l_2}(\mathbf{r}_2)\right], \tag{5}$$

where $\hat{A}_{12}$ is the antisymmetrization operator and $C_{000}^{l_1 l_2 L}$ is the Clebsch–Gordan coefficient that ensures $M_L = 0$ [26]. Projection of the above zero-order basis states onto Equation (3) leads again to a matrix diagonalization problem, the solution of which provides the CI energies, E, and CI coefficients, $C_a^{(EL)}$. The physical interpretation of the coefficient is that $|C_a^{(EL)}|^2$ represents the contribution of the (un-correlated) configuration, Φ_a^L (characterized by the set $'a = (n_1 l_1; n_2 l_2)'$), in the formation of the CI state, Ψ_{EL}, with energy E and angular momentum number L.

2.2. Two- and Three-Photon Ionization Cross Section Formulation

According to LOPT, the N-photon partial-wave ionization cross section, following the absorption of N photons of energy ω, from a system in its ground state $|g\rangle$ (of energy E_g) to a final continuum state of energy E and angular momentum L, is given by [10,27]:

$$\sigma_L^{(N)}(\omega) = 2\pi(2\pi\alpha)^N \omega^N |M_{E_L}^{(N)}|^2 \, \delta(E - E_g - N\omega), \tag{6}$$

where α is the fine structure constant. The total N-photon cross section is given by $\sigma_N(\omega) = \sum_L \sigma_L^{(N)}(\omega)$. The N-photon transition amplitude, $M_{E_F L_F}^{(N)}$, in the case of two-photon absorption, $N = 2$, reduces to:

$$M_{E_L}^{(2)} = \sum\!\!\!\!\!\!\int_{E'_P} \frac{D_{g;E'_P} D_{E'_P;E_L}}{E_g + \omega - E'_P}, \qquad L = S, D, \tag{7}$$

while for three-photon absorption, $N = 3$, it is given by:

$$M_{E_P}^{(3)} = \sum\!\!\!\!\!\!\int_{E'_P} \frac{D_{g;E'_P}}{E_g + \omega - E'_P} \left[\sum\!\!\!\!\!\!\int_{E'_S} \frac{D_{E'_P;E'_S} D_{E'_S;E_P}}{E_g + 2\omega - E'_S} + \sum\!\!\!\!\!\!\int_{E'_D} \frac{D_{E'_P;E'_D} D_{E'_D;E_P}}{E_g + 2\omega - E'_D} \right], \tag{8}$$

$$M_{E_F}^{(3)} = \sum\!\!\!\!\!\!\int_{E'_P} \sum\!\!\!\!\!\!\int_{E'_D} \frac{D_{E_g;E'_P} D_{E'_P;E'_D} D_{E'_D;E_F}}{(E_g + \omega - E'_P)(E_g + 2\omega - E'_D)}, \tag{9}$$

where $D_{E_L;E'_{L'}} \equiv \langle \Psi_{EL} | \hat{D} | \Psi_{E'L'} \rangle$ is the two-electron dipole matrix element and $\Psi_{EL} = \Psi_{EL}(\mathbf{r}_1, \mathbf{r}_2)$ is the CI two-electron eigenstate given by Equation (4). The integrals over the angular symmetries include both the bound and continuum states. The length form of the interaction operator is $\hat{D} = -\hat{e}_p \cdot (\mathbf{r}_1 + \mathbf{r}_2)$ and the velocity form is $\hat{D} = \hat{e}_p \cdot (\nabla_1 + \nabla_2)/\omega$, with $\hat{e}_p$ representing the polarization unit vector of the radiation. The detailed expressions of the dipole matrix elements in terms of the calculated CI two-electron wavefunctions can be found in Ref. [23].

At this point, it is appropriate to comment on the adoption of the dipole approximation used in evaluating transition amplitudes. In the present context of the X-ray regime, the use of the dipole approximation is justified by considering the scaling of the dipole transitions of the one-electron (hydrogenic) systems (see Equation (2)). The mean distance of the electron from the ionic core scales with the nuclear charge, Z, as $\langle r \rangle \sim 1/Z$, while the ionization potential scale as $IP(Z) \sim Z^2$. In the present work, we assume transitions with X-ray photons below the first ionization threshold, $\omega < |E(1s) - E(1s^2)|$. Since generally $|E(1s) - E(1s^2)| < IP(Z)$, we thus have $\omega < Z^2$. The dipole approximation is based on the validity of $|\mathbf{k}_\gamma \cdot \mathbf{r}| << 1$, where $\mathbf{k}_\gamma$ is the wavevector of the X-ray photon and $\mathbf{r}$ the electron's position. From the above considerations, we then have $|\mathbf{k}_\gamma \cdot \mathbf{r}| \simeq k_\gamma \langle r \rangle = \omega \langle r \rangle / c \sim Z^2/(Zc) = Z/c << 1$, for all $Z = 3, 10, 18$ that we consider here ($c \simeq 137.036$).

The angular momentum of the final states, following photoabsorption ($L = 0, 2$ for two-photon absorption and $L = 1, 3$ for three-photon absorption), is dictated by the selection rules implicit in the dipole matrix element. For the present case of linearly polarized light, we have $\Delta M_L = 0$ and $\Delta L = \pm 1$ [26]. Since we start from the ion's ground state ($M_L = 0$), we only need to keep the transitions between the $M_L = 0$ states.

3. Results and Discussion

In Table 1, we give information related to the CI basis used for the various symmetries ^1S,^1P,^1D and ^1F. The configuration states, $\Phi_{n_1 l_1; n_2 l_2}^{(L)}(\mathbf{r}_1, \mathbf{r}_2)$, have been constructed according to Equation (5) by one-electron orbitals with angular momenta given in Table 1 and energies sufficiently high to ensure convergence of the results. The order of B-splines was $k_b = 9$ with the total number of

B-spline polynomials set at $n_b = 110$ for Li^+ and $n_b = 170$ for Ne^{9+} and Ar^{16+}. The box radius varied between $R = 50 - 58$ a.u. for Li^+, $R = 20 - 28$ a.u. for Ne^{8+} and $R = 10 - 15$ a.u. for Ar^{16+}. The knot sequence of the spatial grid for the B-spline basis was linear. The two-electron wavefunctions, $\Phi^{(L)}_{n_1 l_1, n_2 l_2}(\mathbf{r}_1, \mathbf{r}_2)$, have been constructed from the zero-order configurations by one-electron orbitals with angular momenta given in the mentioned table and energies determined by the indices n_1, n_2 in the following ranges: $1 \leq n_1 \leq 6$ and $1 \leq n_2 \leq n_b$. The relationship of the indices n_1, n_2 to the energies of the zero-order wavefunctions depends on the basis size parameters such as the maximum value of the box radius as well as the number of B-spline basis functions used. In summary, the whole basis, for each symmetry, resulted in the inclusion of the following number of functions for each ion: 1650–1940 for Li^+, 1600 for Ne^{8+} and 2040 for Ar^{16+}.

Table 1. (l_1, l_2) electronic configurations included in the configuration interaction (CI) calculations for the ^1L symmetries.

^1S	^1P	^1D	^1F
s^2	sp	sd	sf
p^2	pd	p^2	pd
d^2	df	pf	pg
f^2	fg	d^2	df
g^2		dg	fg
		f^2	

In Table 2, we show the calculated energies for a few lower bound states of the hydrogenic ions Li^{2+}, Ne^{9+} and Ar^{17+}. The degree of the agreement with those reported in the National Institute of Standards and Technology (NIST) atomic spectra database [28] is given in the last row of the table. In all cases, the percentage discrepancies of the ground state energies (between the calculated and those of the NIST database) are of the order 0.1% while the excited states are of similar or even smaller order.

Table 2. Energies of the few lowest states of the one-electron Li^{2+}, Ne^{9+} and Ar^{17+} ions. Energies are given in units of eV. Energies are relative to the single-ionization threshold. $\delta E(1s) \equiv |E(1s) - E_g^{Z+}|/|E_g^{Z+}|$ is the relative discrepancy (between our calculated ground state values with the energies (E_g^{Z+}) listed in the NIST database [28]). The relative discrepancy for excited states is generally less than $\delta E(1s)$.

State	Li^{2+}	Ne^{9+}	Ar^{17+}
$1s$	-122.451	-1360.57	-4408.2
$2s, 2p$	-30.613	-340.14	-1102.1
$3p, 3d$	-13.606	-151.18	-489.8
$4d, 4f$	-7.653	-85.04	-275.5
$5f$	-4.898	-54.42	-176.3
$\delta E(1s)$	2.5×10^{-5}	1.2×10^{-3}	4.1×10^{-3}

In Table 3, we show the energy differences of the few lowest states of Li^+, Ne^{8+} and Ar^{16+} ions with respect to the respective ground state ($1s^2\ ^1S_0$) energy of each ion. In all cases, the percentage discrepancies of the ground state energies (between the calculated and those of the NIST) are of the order 0.1% while the excited states are of similar or even of smaller order. This is not surprising as the role of correlation is more important in the lower energy states, where the electrons are on average closer relative to the higher-energy states.

Having examined the reliability of the calculated electronic structure, within the available theoretical and experimental data to compare, we proceed to the main subject of this work: the presentation of ionization cross sections for a range of photon frequencies. In all the following, the horizontal axis in the figures represents the photon energy, given in eV. The cross sections are

given in SI units, $\mathrm{cm}^{2N}\mathrm{s}^{N-1}$, where N is the order of the process (here equivalent with the number of the photons absorbed). The final angular momenta, following two-photon absorption are the ^1S,^1D continua, while in the case of three-photon absorption are the ^1P,^1F continua. The cross sections have been evaluated using both the length and the velocity forms of the dipole operator. They generally have excellent agreement throughout all the spectral regions considered, especially for the non-resonant ones. Relative agreement between the length and the velocity forms is important since it provides strong evidence that the dipole matrix elements, contributing in the multiphoton transition amplitude, have been converged.

Table 3. Energy differences of the few lowest states of Li^+, Ne^{8+} and Ar^{16+} ions with respect to their respective ground state ($1s^2\ ^1S_0$) energy value. We use boldface for the states' notation to emphasize that they are listed according the dominant configuration in the CI expansion of Equation (4). In the last row, $\delta E(1s^2) \equiv |E(1s^2) - E_g^{Z+}|/|E_g^{Z+}|$ is the relative discrepancy (between our calculated ground state values and the energies (E_g^{Z+}) listed in the NIST database [28]). $E(1s^2)$ is given relative to the double ionization threshold.

State	**Li^+**	**Ne^{8+}**	**Ar^{16+}**
$1s2s$	60.42	914.0	3114.1
$1s2p$	61.67	920.4	3126.7
$1s3s$	68.73	1070.1	3666.1
$1s3d$	69.02	1071.5	3668.7
$1s3p$	69.09	1072.0	3669.7
$1s4s$	71.54	1124.5	3858.7
$1s4d$	71.66	1125.1	3859.9
$1s4p$	71.67	1125.3	3860.2
$1s4f$	71.67	1125.1	3859.8
$1s5s$	72.83	1149.6	3947.7
$1s5d$	72.89	1148.9	3948.3
$1s5p$	72.90	1150.0	3948.5
$1s5f$	72.89	1149.9	3948.3
$E(1s^2)$	-197.518	-2554.53	-8513.84
$\delta E(1s^2)$	2.9×10^{-3}	1.36×10^{-3}	3.87×10^{-3}

In Figures 1–3, we show the photon energy dependence of the calculated two photon partial-ionization cross sections, $\sigma_S^{(2)}(\omega), \sigma_D^{(2)}(\omega)$, of Li^+, Ne^{8+} and Ar^{16+}, respectively, from the ground state, $1s^2(^1S)$, to final states of symmetry ^1S, ^1D. Summing the latter, we obtain the corresponding total two-photon ionization cross sections, $\sigma_2(\omega)$. For clarity, we have plotted only the length-form results. Generally, for all three ions, the dominant two-photon ionization channel is the ^1D symmetry. The cross sections exhibit strong peak structures, which appear in both the ^1S and ^1D final symmetries, due to one-photon resonance with the intermediate states $1snp\ ^1P, n = 2, 3, ...$ Apart from these intermediate-resonance peaks, there are further peaks due to strong configuration mixing of the type $npn'p$, $n, n' = 2, 3...$, associated with the ^1S, ^1D continua.

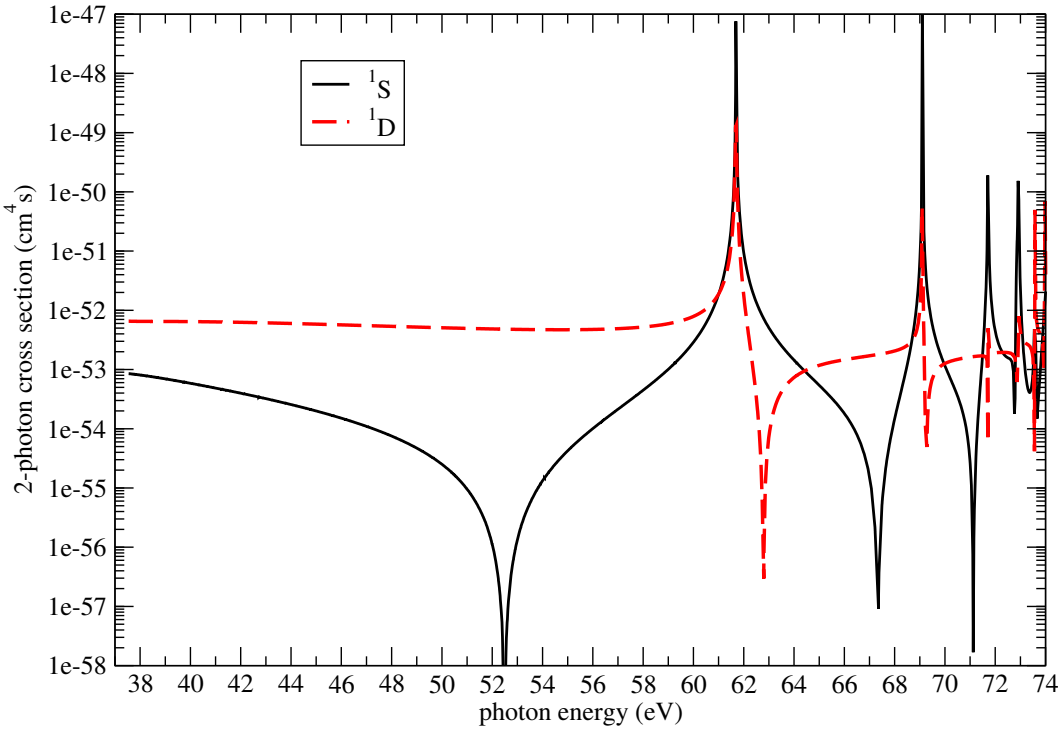

Figure 1. Two-photon partial ionization cross sections of Li^+ from its ground state with linearly polarized light. The characteristic peaks in the cross section are associated with the intermediate bound states of the symmetry ^1P.

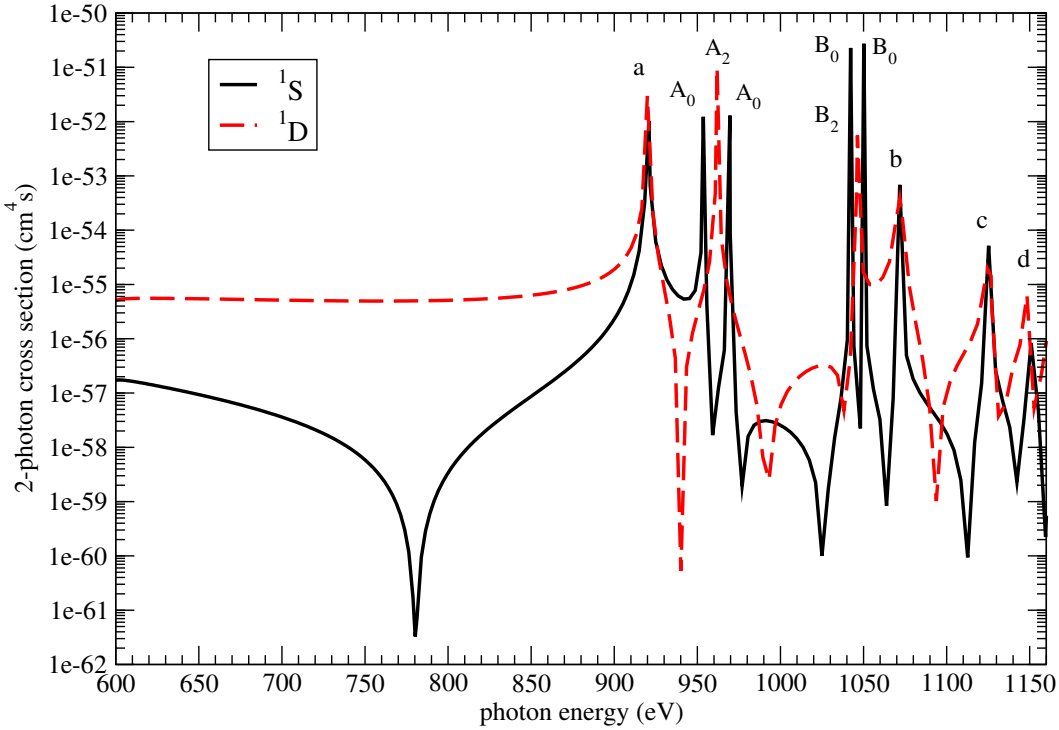

Figure 2. Two-photon partial ionization cross sections of Ne^{8+} from its ground state with linearly polarized light. The small letters (a, b, c) indicate features associated with the intermediate bound states of symmetry ^1P while the capital letters $(A_i, B_i, i = 0, 2)$ are associated with final state correlations.

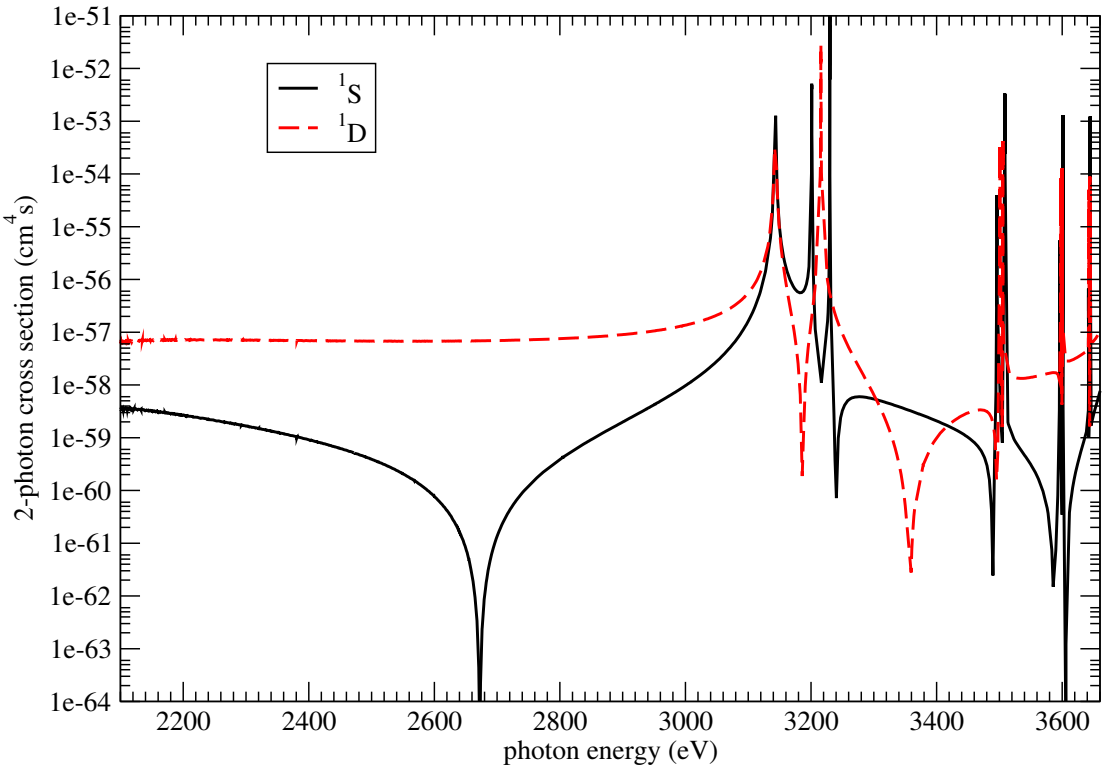

Figure 3. Two-photon partial ionization cross sections of Ar^{16+} from its ground state with linearly polarized light.

The configuration-mixing peaks are absent for two-photon ionization of Li^+ ionization since these would occur at higher photon energy, past about 75 eV, as the lowest post-ionization energy levels are about 150 eV and half that value (two photons) is about 75 eV. When we add the ^1S and ^1D cross sections to obtain the total cross section, we find a relatively good agreement with that of Ref. [15], which models two-photon ionization of Li^+ employing a less elaborate approach, namely, single-channel quantum defect theory; when our shift is accounted for, our peaks occur close to that work (62.2 eV $1s2p(^1P)$, 69.7 eV $1s3p(^1P)$, 72.3 eV $1s4p(^1P)$ and 73.5 eV $1s5p(^1P)$), and our (partial-wave sum) cross section baseline between 50–55 eV is within the same order of magnitude as in Ref. [15] (both between 10^{-53}–10^{-52} cm^4·s); however, our shape is slightly different here, being slightly convex (downward) in this region.

For Ne^{8+} and Ar^{16+}, our values are also in good agreement with the Green-function calculations in Ref. [18]. In addition, for Ne^{8+}, we have also compared our values with the second-order perturbation theory calculation of Novikov and Hopersky [16]; their $1s2p(^1P)$ and $1s3p(^1P)$ one-photon resonance peaks (these are their only peaks) are comparable to ours occurring at around 920 eV and 1070 eV, respectively. Their cross section base-line (non-resonant part) circa 600–800 eV is also close to ours, i.e., within the same order of magnitude (both between 10^{-56}–10^{-55} cm^4·s).

In relation to the intermediate resonance peaks in Table 3, we show the energy differences of the few lowest states of Li^+, Ne^{8+} and Ar^{16+} ions from their respective ground state ($1s^2\ ^1S_0$) energy, $E_g = E_{1s^2}$, namely, $\Delta E_P \equiv E_P - E_g$, (i.e., corresponding to peaks (a–d) in Figure 2). Their importance is derived from the fact that these energy differences appear in the denominator of the two-photon cross section expression, Equation (7), i.e., $E_g + \omega - E'_P = \omega - \Delta E_P$. It is then immediately evident that the photon energy detuning from these energy differences generates a series of characteristic features in the cross section. A word of caution is necessary at this point: within the current formulation, the height of these peaks becomes infinite in the exact on-resonance case, $\Delta E_P = \omega$. The first point to note is that we have ignored the inherent spontaneous decay width of the intermediate bound states. This would have served only to remove the unphysical singularities that occur at the resonances

positions. However, most importantly, the LOPT cross sections fail to provide the correct ionization yields. In other words, in the resonant case, the LOPT relation for the ionization yield,

$$W_{gf} = \sigma_N F^N, \tag{10}$$

(F is the pulse's flux) becomes invalid. It is well established that, for resonant and near-resonant processes, while perturbation theory is still valid, an alternative formulation is required for the calculation of the expected ionization yields. This formulation, in addition to the ionization of the system directly from the ground state, takes into account the stepwise formation and the subsequent ionization of the intermediate states. Without going into the details, we shall only mention that in such cases the formulation should be developed in terms of a density matrix representation in combination with a proper representation of the spatiotemporal profile of the laser field. At this point, it is worth noting the pulse properties for which the LOPT cross sections presented here are valid. Equation (10) is only just marginally applicable for a pulse with its detuning from a resonance of the same order as its bandwidth, $\Delta E_P \sim \gamma_L$, where γ_L is the bandwidth. If we take as a rough rule that the bandwidth of the pulse is, say, a 1/100-th of its average photon energy ($\gamma_L \sim \omega/100$), that would mean that the cross section values within the range 61.47 ± 0.61 eV (first peak in the two-photon cross section for Li^+) cannot be safely used in combination with Equation (10). Similar considerations should be assumed for the higher peaks. For completeness, for Ne^{8+} and Ar^{16+}, if based again on the appearance of the first peaks in the two-photon cross section (see the first row for the $1s2p$ state in Table 3), the corresponding intervals are scaled upwards to ± 9.2 eV ($\sim 920/100$) and ± 31 eV ($\sim 3126/100$), respectively. A case that such a discrepancy between the LOPT two-photon ionization cross section [16] and the experimental value [29] is attributed to the bandwidth of the X-ray pulse can be found in Ref. [17]. More specifically, for an X-ray photon energy of 1110 eV (in between (b) and (c) peaks in Figure 2), the reported experimental value was 7×10^{-54} cm^4·s [29] while the theoretical cross section based on a Hartree–Fock–Slater (HFS) model was found to be equal to 4.0×10^{-57} cm^{4}s. Our calculated value for this photon energy is about 4.6×10^{-57} cm^{4}s for the ^1D wave while the ^1S value makes a negligible contribution to the total cross section.

For Ne^{8+} and Ar^{16+}, the 'twin' peaks (see A_0 peaks in Figure 2), exclusive to the ^1S symmetry, are due to the strong coupling between the $2s2s$ and $2p2p$ configurations in the expansion Equation (4). Since in the ^1D symmetry the $2s2s$ configuration is missing, we observe only one peak (A_2 in Figure 2), in between the A_0 ones. To confirm this, we have performed some further tests where, for example, we excluded the $\Phi^{^1S}_{2s2s}$, $\Phi^{^1S}_{2p2p}$ zero-order states (separately each time) from the CI wavefunction, Equation (4). By doing this, we obtain a cross section with only one A_0 peak at the same position where the A_2 peak appears. This suggests that the observed (two) A_0 peaks are the result of strong-mixing of the $2s2s$ and $2p2p$ configurations, mainly due to their proximity in energy.

Similar considerations hold for the peaks B_0, B_2 at higher photon energies. The B_0 twin peaks are due to the mixing of the Φ_{2s3s},Φ_{2p3p} configurations in the ^1S symmetry, while the B_2 peak is due to the $3p^2$ state exclusively. We mention here that these doubly excited (highly correlated) states are also known as autoionizing states as they are associated with a temporal trap of the two excited electrons in the core's region, eventually leading to the ejection of one of them and the residual (higher-charged ion) to its ground state. In the present (static) context of the CI calculation, these doubly excited states are degenerate with the $1s^2\,^1S$ or $1sd\,^1D$ continua, which eventually cause their radiationless (auto)-ionization [30].

In Figures 4–6, we present our calculated three photon partial-ionization cross sections of Li^+, Ne^{8+} and Ar^{16+}, respectively, from the ground state $1s^2(^1S)$. The final angular momentum of the ions, following three-photon absorption, are the ^1P,^1F continua, all being of singlet symmetry. Similarly, as in the two-photon case, the total three-photon ionization cross section is obtained by the addition of the ^1P and ^1F partial-wave cross sections. Again, the final state is dominated by configurations with the residual ion in its ground state and the ejected electron with angular momentum $l = 1$ for the ^1P and $l = 3$ for the ^1F symmetry. The three-photon cross sections exhibit strong peak

structures, which appear in both ^1P and ^1F final symmetries, due to two-photon resonances with the intermediate states $1s3d, 1s4d, ...$ (see denominators $(E_g + 2\omega - E_L, L = S, D)$ in Equations (8) and (9)). In the ^1P symmetry, there are additional peaks due to two-photon resonance states of the type $1sns\,^1S, n = 2, 3, ...$ Because the $1s3s$ and $1s3d$ states have slightly different energy positions, the intermediate resonance peaks for the ^1P and ^1F (for example circa 34.4 eV for Li^+) do not generally coincide. Note that the ^1P final states are reached by the coherent superposition of two ionization absorption channels: $S \to P \to S \to P$ and $S \to P \to D \to P$. In contrast, the ^1F states are reached only via one ionization channel, namely: $S \to P \to D \to F$.

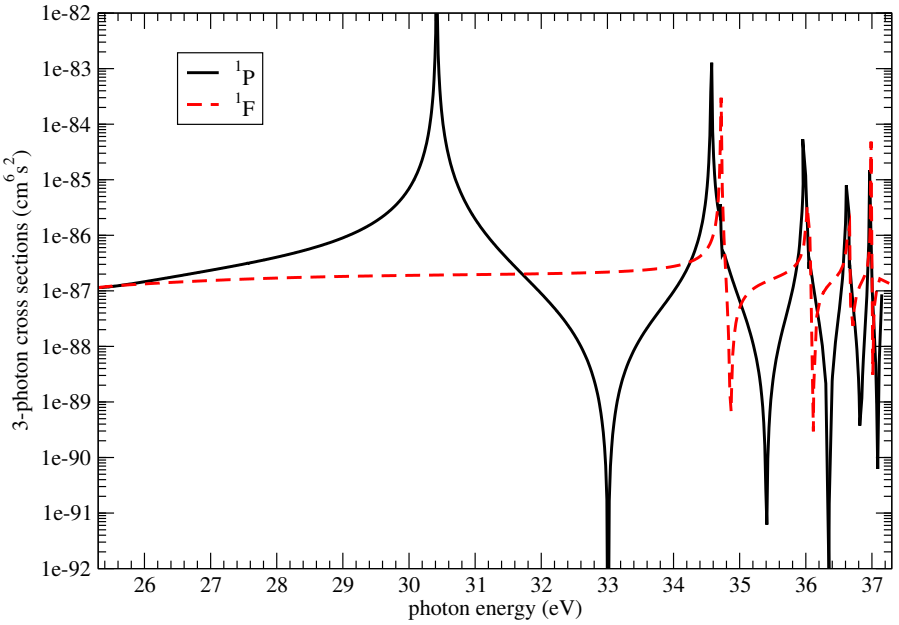

Figure 4. Three-photon ionization partial cross sections of Li^+ from its ground state with linearly polarized light.

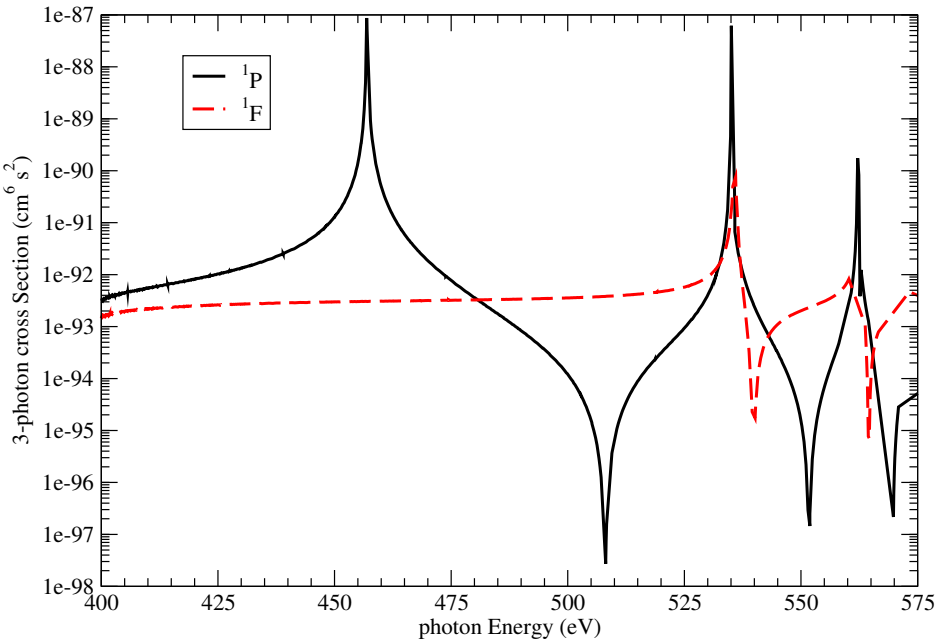

Figure 5. Three-photon ionization partial cross sections of Ne^{8+} from its ground state with linearly polarized light.

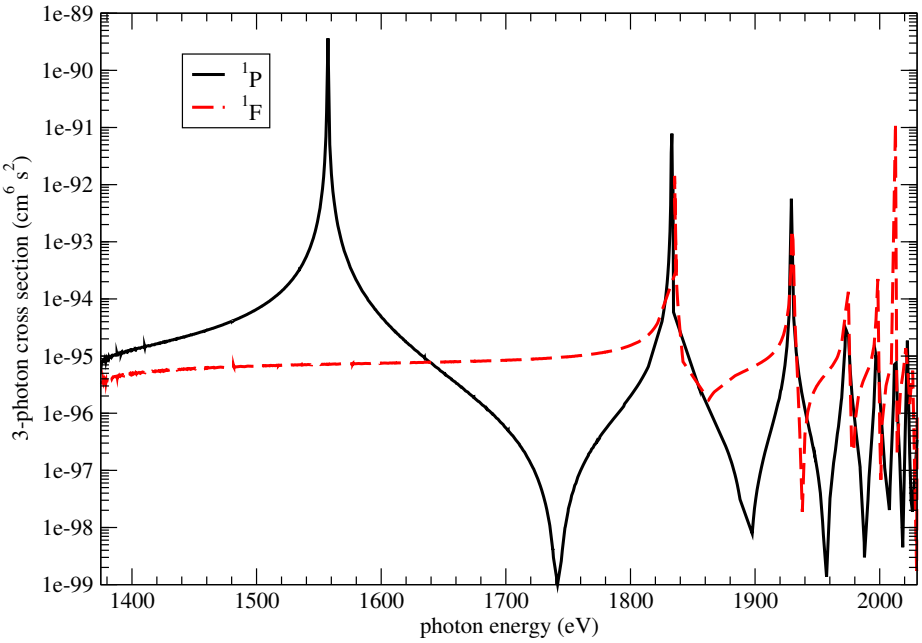

Figure 6. Three-photon ionization partial cross sections of Ar^{16+} from its ground state with linearly polarized light.

At this point, it might be worth comparing the cross sections among the three investigated ions. It is clearly visible from the figures that generally the ionization cross section decreases from Li^+ towards Ar^{16+}. This observation is rather consistent with the (exact) scaling, $1/Z^{4N-2}$, of the N-photon cross section for hydrogenic systems [11]. A second point worth mentioning is that the cross sections ending on the higher symmetry, ^1D for two-photon and ^1F for three-photon ionization, are proportional to the cross sections for circularly polarized light. To be more specific, due to the dipole selection rules, ionization by circularly polarized light will proceed through intermediate states where M_L will change either by $+1$ or by -1 monotonously. For example, let us assume circularly polarized light which causes a change of the magnetic quantum number by $\Delta M_L = +1$. This means that if we start from the ground state, where $L = 0$ and $M_L = 0$, then the first ionization step will involve only states with $M_L = +1$. Similarly, the next ionization step will involve states that differ by $+1$ from the previous step, meaning that only states with $M_L = +2$ will be accessed in this step. In this case, these states will necessarily have $L = 2$. Accordingly, if further ionization occurs (three-photon ionization), for the same reason, only states with $M_L = +3$ will be reached, thus ending necessarily with an $L = 3$ total orbital angular momentum. Similar considerations hold had we started by circularly polarized light with opposite helicity, leading to a change of $\Delta M_L = -1$. In short, for two-photon ionization, only the ionization path $S \to P \to D$ is allowed. Accordingly, for three-photon ionization, only the $S \to P \to D \to F$ ionization channel will occur. Now the crucial observation is that the transition amplitudes by circularly and linearly polarized light for these ionization paths differ only by the total magnetic quantum number, M_L. For linearly polarized light, it is $\Delta M_L = 0$, while for circularly polarized light, it is $|\Delta M_L| = 1$. Straightforward angular momentum algebra for these transition amplitudes ($T_C(T_L)$ for circular(linear)-polarized light) of two-electron states shows that they differ only by a proportional factor; namely, $|T_C(D)/T_L(D)| = \sqrt{3/2}$ for two-photon ionization and $|T_C(F)/T_L(F)| = \sqrt{5/2}$, for three-photon ionization, where D and F denote the final angular momentum channel for two-photon and three-photon ionization, respectively [31]. Nevertheless, note that circularly polarized light does not guarantee that the total ionization cross section will provide higher rates relative to the ionization by linearly polarized light; the final rate depends on the number of available ionization paths available and the electric field intensity and, in fact, high N-photon ionization by linearly polarized light is more effective.

4. Conclusions

In conclusion, motivated by the wide array of X-ray facilities worldwide that are able to investigate nonlinear interactions with atomic systems on their natural time scales, we have presented calculations for two- and three-photon partial ionization cross sections of Li^+, Ne^{8+} and Ar^{16+} ions. These systems are of high experimental and theoretical interest for the study of interaction of strong and ultrashort X-ray radiation at a fundamental level. We have identified that the ionization cross sections are dominated by a series of intermediate (one or two-photon) resonance peaks in addition to peaks due to doubly excited structures. We have noticed the trend that from the lower Z ion, Li^+, to the higher ones, the ionization cross sections generally decrease.

Acknowledgments: This work was supported by the Science Foundation Ireland under Grant No. 12/IA/1742 and enabled by the EU Education, Audio-visual and Culture Executive Agency (EACEA) Erasmus Mundus Joint Doctorate Programme EXTATIC, Project No. 2013-0033. This work is also associated with the FP7 EU COST Actions MP1203 and CM1204.

Author Contributions: W.H. carried out the calculations and analysed the results. J.T.C. co-supervised W.H. L.A.A.N. supervised W.H. and the project, developed the code and contributed to the analysis of the results. W.H., J.T.C. and L.A.A.N. wrote the paper.

Conflicts of Interest: The authors declare no conflict of interest.

References

1. Glover, T.; Hertlein, M.P.; Southworth, S.H.; Allison, T.K.; van Tilborg, J.; Kanter, E.P.; Krässig, B.; Varma, H.R.; Rude, B.; Santra, R.; et al. Controlling X-rays with light. *Nat. Phys.* **2010**, *6*, 69–74.
2. Tamasaku, K.; Nagasono, M.; Iwayama, H.; Shigemasa, E.; Inubushi, Y.; Tanaka, T.; Tono, K.; Togashi, T.; Sato, T.; Katayama, T.; et al. Double Core-Hole Creation by Sequential Attosecond Photoionization. *Phys. Rev. Lett.* **2013**, *111*, 043001.
3. Young, L.; Kanter, E.P.; Krässig, B.; Li, Y.; March, A.M.; Pratt, S.T.; Santra, R.; Southworth, S.H.; Rohringer, N.; DiMauro, L.F.; et al. Femtosecond electronic response of atoms to ultra-intense X-rays. *Nature* **2010**, *466*, 56–61.
4. Fukuzawa, H.; Son, S.-K.; Motomura, K.; Mondal, S.; Nagaya, K.; Wada, S.; Liu, X.-J.; Feifel, R.; Tachibana, T.; Ito, Y.; et al. Deep Inner-Shell Multiphoton Ionization by Intense X-ray Free-Electron Laser Pulses. *Phys. Rev. Lett.* **2013**, *110*, 173005.
5. Ghimire, S.; Fuchs, M.; Hastings, J.; Herrmann, S.C.; Inubushi, Y.; Pines, J.; Shwartz, S.; Yabashi, M.; Reis, D.A. Nonsequential two-photon absorption from the *K* shell in solid zirconium. *Phys. Rev. A* **2016**, *94*, 043418.
6. Costello, J.; Kennedy, E.; Nikolopoulos, L. Short wavelength free electron lasers. *J. Mod. Opt.* **2016**, *63*, 285–287.
7. Pellegrini, C.; Marinelli, A.; Reiche, S. The physics of X-ray free-electron lasers. *Rev. Mod. Phys.* **2016**, *88*, 015006.
8. Bostedt, C.; Boutet, S.; Fritz, D.; Huang, Z.; Lee, H.; Lemke, H.; Robert, A.; Schlotter, W.; Turner, J.; Williams, G. Linac Coherent Light Source: The first five years. *Rev. Mod. Phys.* **2016**, *88*, 015007.
9. Falcone, R.; Dunne, M.; Chapman, H.; Yabashi, M.; Ueda, K. Frontiers of free-electron laser science II. *J. Phys. B* **2016**, *49*, 180201.
10. Lambropoulos, P. Topics on multiphoton processes. *Adv. At. Mol. Phys.* **1976**, *12*, 87–164.
11. Madsen, L.; Lambropoulos, P. Scaling of hydrogenic atoms and ions interacting with laser fields: Positronium in a laser field. *Phys. Rev. A* **1999**, *59*, 4574–4579.
12. Karule, E. On the evaluation of transition matrix elements for multiphoton processes in atomic hydrogen. *J. Phys. B* **1971**, *4*, L67.
13. Potvliege, R.M.; Shakeshaft, R. High-order above-threshold ionization of hydrogen in perturbation theory. *Phys. Rev. A* **1989**, *39*, 1545–1548.
14. Saenz, A.; Lambropoulos, P. Theoretical two-, three- and four-photon ionization cross sections of helium in the XUV range. *J. Phys. B* **1999**, *32*, 5629.
15. Emmanouilidou, A.; Hakobyan, V.; Lambropoulos, P. Direct three-photon triple ionization of Li and double ionization of Li^+. *J. Phys. B* **2013**, *46*, 111001.

16. Novikov, S.A.; Hopersky, A.N. Two-photon excitation-ionization of the 1s shell of highly charged positive atomic ions. *J. Phys. B* **2001**, *34*, 4857–4863.
17. Sytcheva, A.; Pabst, S.; Son, S.; Santra, R. Enhanced nonlinear response of Ne8+ to intense ultrafast X-rays. *Phys. Rev. A* **2012**, *85*, 023414.
18. Koval, P. Two-Photon Ionization of Atomic Inner-Shells. Ph.D. Thesis, University of Kassel, Kassel, Germany, 2004.
19. Chang, T.; Kim, Y. Theoretical study of the two-electron interaction in alkaline-earth atoms. *Phys. Rev. A* **1986**, *34*, 2609–2613.
20. Tang, X.; Chang, T.; Lambropoulos, P.; Fournier, S.; DiMauro, L. Multiphoton ionization of magnesium with configuration interaction calculations. *Phys. Rev. A* **1990**, *41*, R5265.
21. Chang, T.; Tang, X. Photoionization of two-electron atoms using a nonvariatonal configuration interaction approach with discretized finite basis. *Phys. Rev. A* **1991**, *44*, 232–238.
22. Chang, T. *Many-Body Theory of Atomic Structure*; Chapter B-Spline Based Configuration-Interaction Approach for Photoionization of Two-Electron and Divalent Atoms; World Scientific: Singapore, 1993; pp. 213–247.
23. Nikolopoulos, L.A.A. A package for the ab initio calculation of one- and two-photon cross sections of two-electron atoms, using a CI B-splines method. *Comput. Phys. Commun.* **2003**, *150*, 140–165.
24. De Boor, C. *A Practical Guide to Splines*; Springer: New York, NY, USA, 1978.
25. Bachau, H.; Cormier, E.; Decleva, P.; Hansen, J.E.; Martin, F. Applications of B-splines in Atomic and Molecular Physics. *Rep. Prog. Phys.* **2001**, *64*, 1815–1942.
26. Sobel'man, I. *Introduction to the Theory of Atomic Spectra*; Pergamon Press Ltd.: Oxford, UK, 1972.
27. Nikolopoulos, L.A.A. Mg in electromagnetic fields: Theoretical partial multiphoton cross sections. *Phys. Rev. A* **2005**, *71*, 033409.
28. Kramida, A.; Yu, R.; Reader, J.; NIST ASD Team. *NIST Atomic Spectra Database (ver. 5.3)*; National Institute of Standards and Technology: Gaithersburg, MD, USA, 2015.
29. Doumy, G.; Roedig, C.; Son, S.-K.; Blaga, C.I.; di Chiara, A.D.; Santra, R.; Berrah, N.; Bostedt, C.; Bozek, J.D.; Bucksbaum, P.H.; et al. Nonlinear atomic response to intense ultrashort X-rays. *Phys. Rev. Lett.* **2011**, *106*, 083002.
30. Fano, U. Effects of Configuration Interaction on Intensities and Phase Shifts. *Phys. Rev.* **1961**, *124*, 1866–1878.
31. Nikolopoulos, L.A.A. Dublin City University, Dublin, Ireland. Unpublished notes.